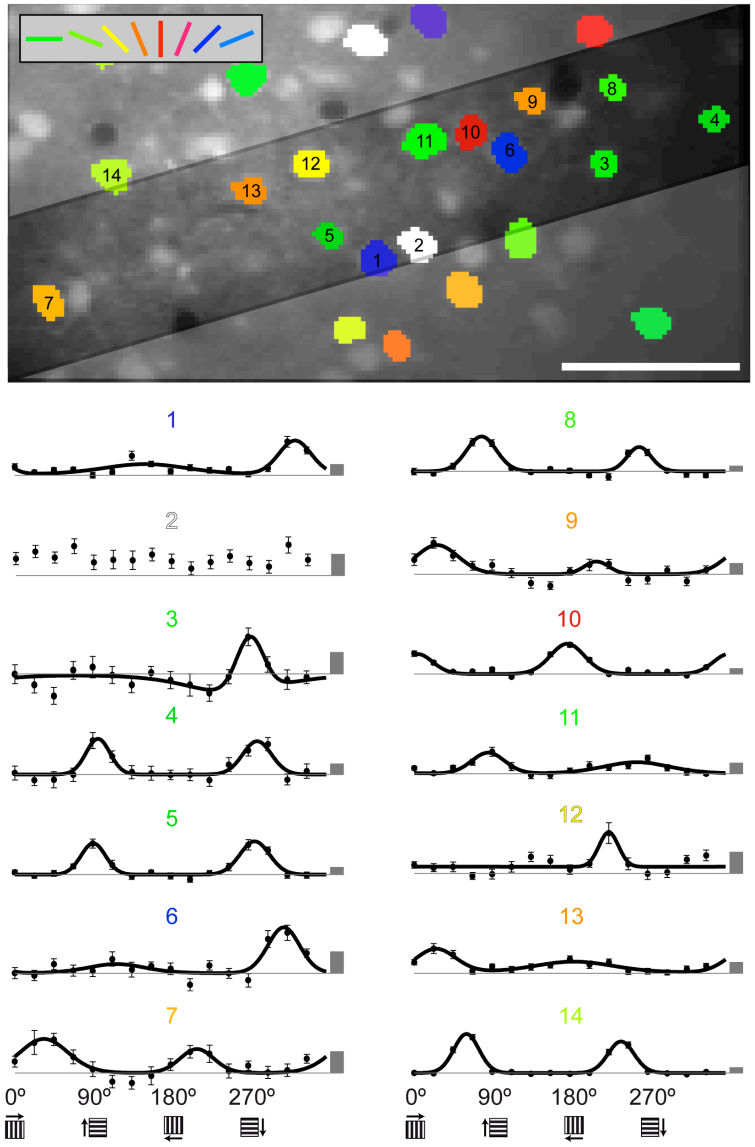


**Supplementary Figure 1. *In vivo* functional properties of neurons in the EM imaged volume.** (Top) Cell-based orientation preference map in mouse visual cortex. (Bottom) Orientation tuning curves of functionally characterized cells contained in the EM volume (dark diagonal band, cell orientation preference coloured as in Fig. 1). Average responses to 16 directions (points) were fit to the sum of two Gaussians (line; see Methods). Responses from cell 2 were non-selective (OSI ≤ 0.2) and therefore not fit. Gray horizontal bars at right indicate 4% ΔF/F. Scale bar, 50 μm. Error bars are +/- SEM.

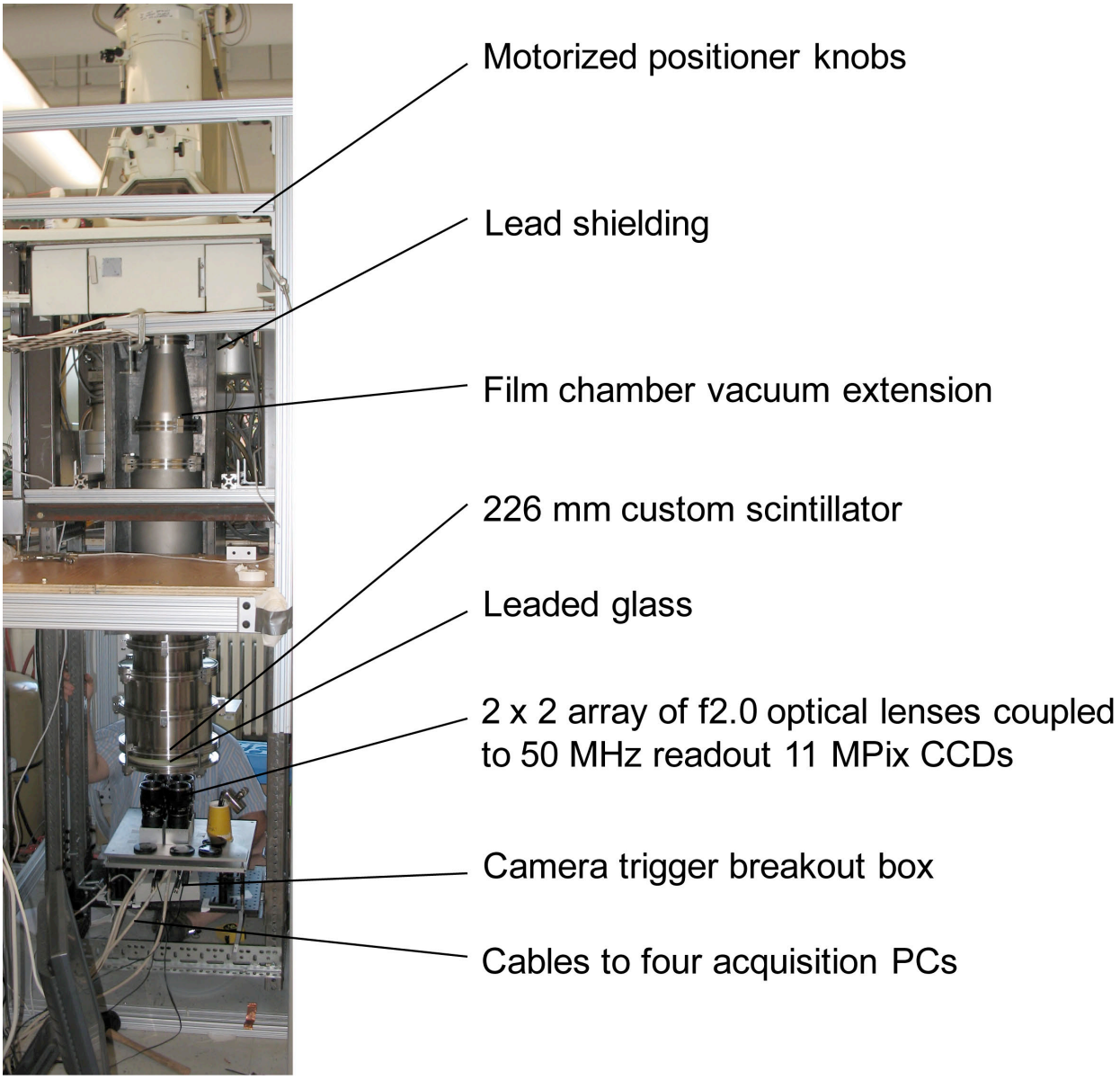


**Supplementary Figure 2. Transmission electron microscope camera array (TEMCA).** Key modifications enabling high-throughput EM image acquisition are labelled.

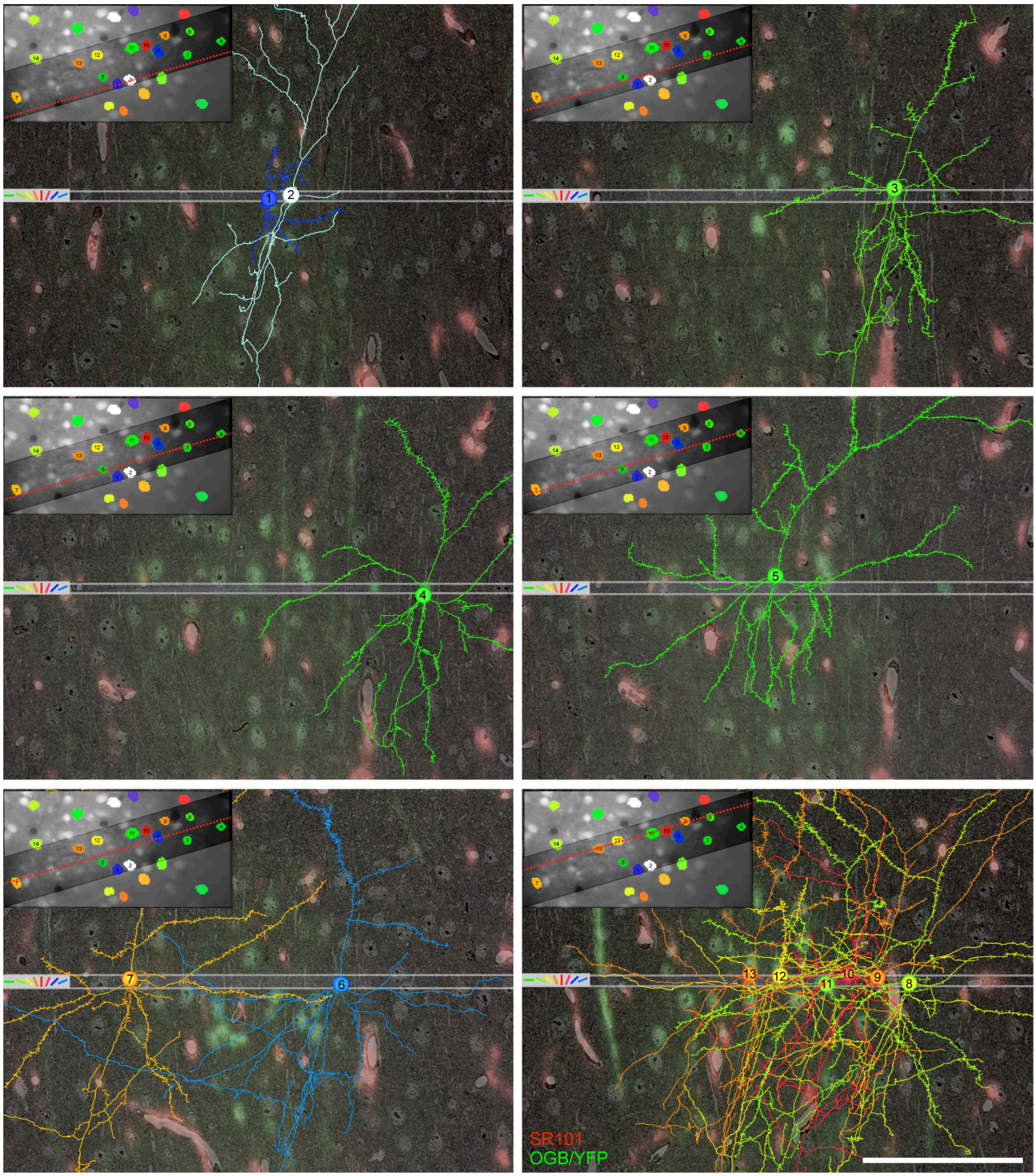


**Supplementary Figure 3. Correspondence between *in vivo* fluorescence anatomy and electron microscopy throughout the EM volume.** Merged *in vivo* fluorescence and single thin section EM data at different positions in the imaged volume, with reconstructions of each functionally characterized cell. Horizontal grey bars bound the

functionally imaged plane. Cell colours represent preferred orientation as in Fig. 1b. Outside the functionally imaged plane, colours represent anatomy as in Fig. 1c (red: blood vessels or astrocytes, green: OGB or YFP). Blood vessels and astrocytes are well registered with SR101 and nuclei are well registered with OGB. Insets show the approximate position (dotted red line) for each orthogonally cut EM section within the functionally imaged plane. Apical dendrites and dendritic spines not participating in connectivity graphs were traced by a small team of students (A. Arons, J. DiMartino, T. Law, M. Pershan, S. Reid, V. Swantic). Scale bar, 100 μm.

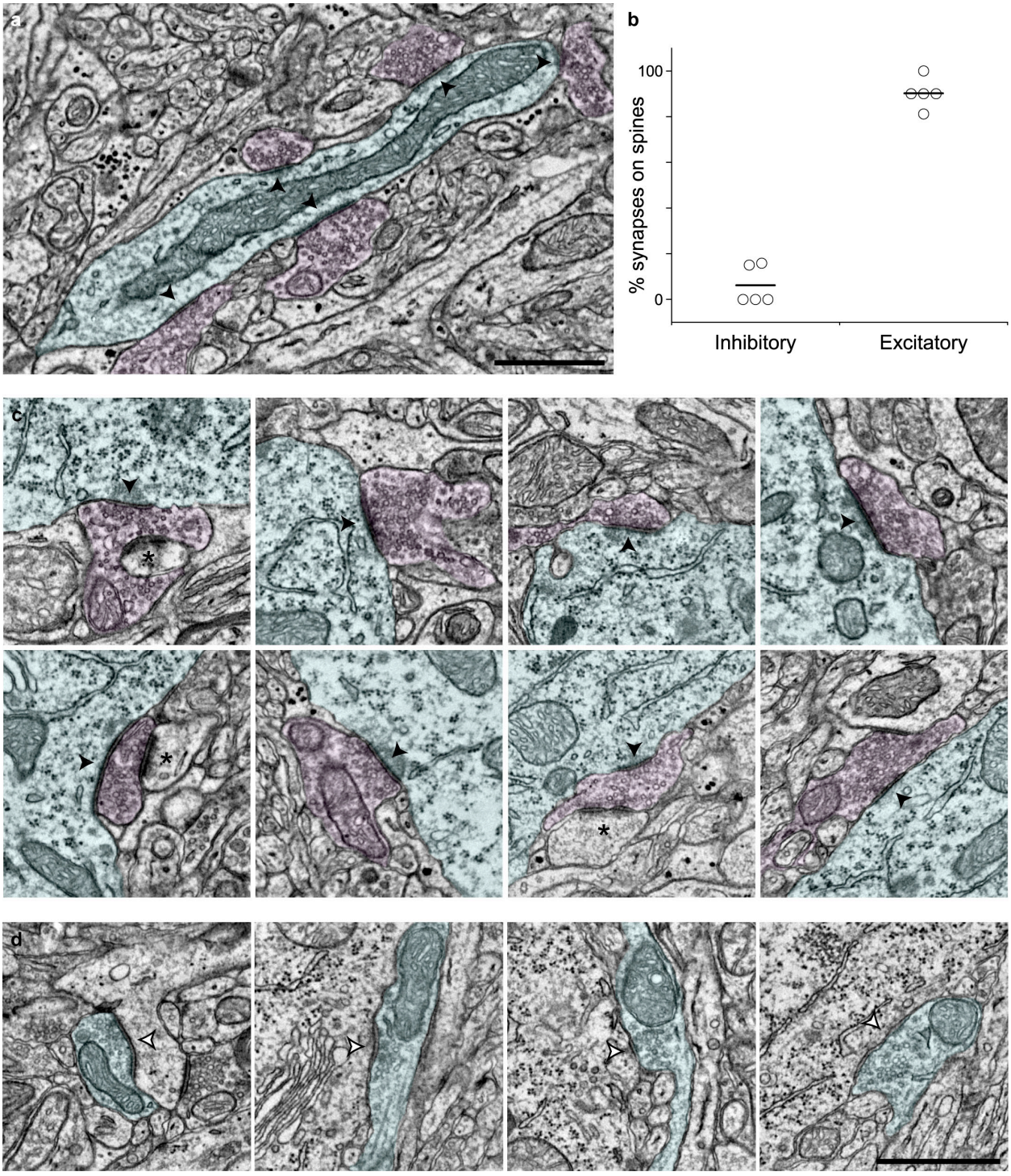


**Supplementary Figure 4. Anatomical hallmarks of cortical inhibitory interneurons.**

**a,** Section through an obliquely cut dendrite of a non-pyramidal interneuron. The interneuron dendrite (cyan) and five excitatory presynaptic terminals (magenta) are

pseudo-coloured. The synaptic terminals were classified as asymmetric and excitatory (Gray's Type 1) by the presence of pronounced postsynaptic densities (solid arrowheads) and round vesicles. Also note the absence of spines on the interneuron dendrite. **b,** Inhibitory and excitatory postsynaptic processes are anatomically distinct. The percentage of synapses occurring on spines for the two classes did not overlap. The horizontal bar indicates the mean. **c,** Interneurons receive asymmetric synapses onto their cell bodies. All 8 interneurons receiving convergent input whose cell bodies (cyan) were contained in the EM volume received multiple asymmetric synapses on the soma; an example synapse (solid arrowhead) is shown from each cell. In several instances the same excitatory presynaptic bouton (magenta) also synapsed onto a nearby dendritic spine (asterisks) of unknown origin. **d,** The axon of the non-stimulus selective interneuron (cell 2) makes symmetric synapses (empty arrowheads) onto its postsynaptic targets; four are shown. Scale bars, 1 μm.

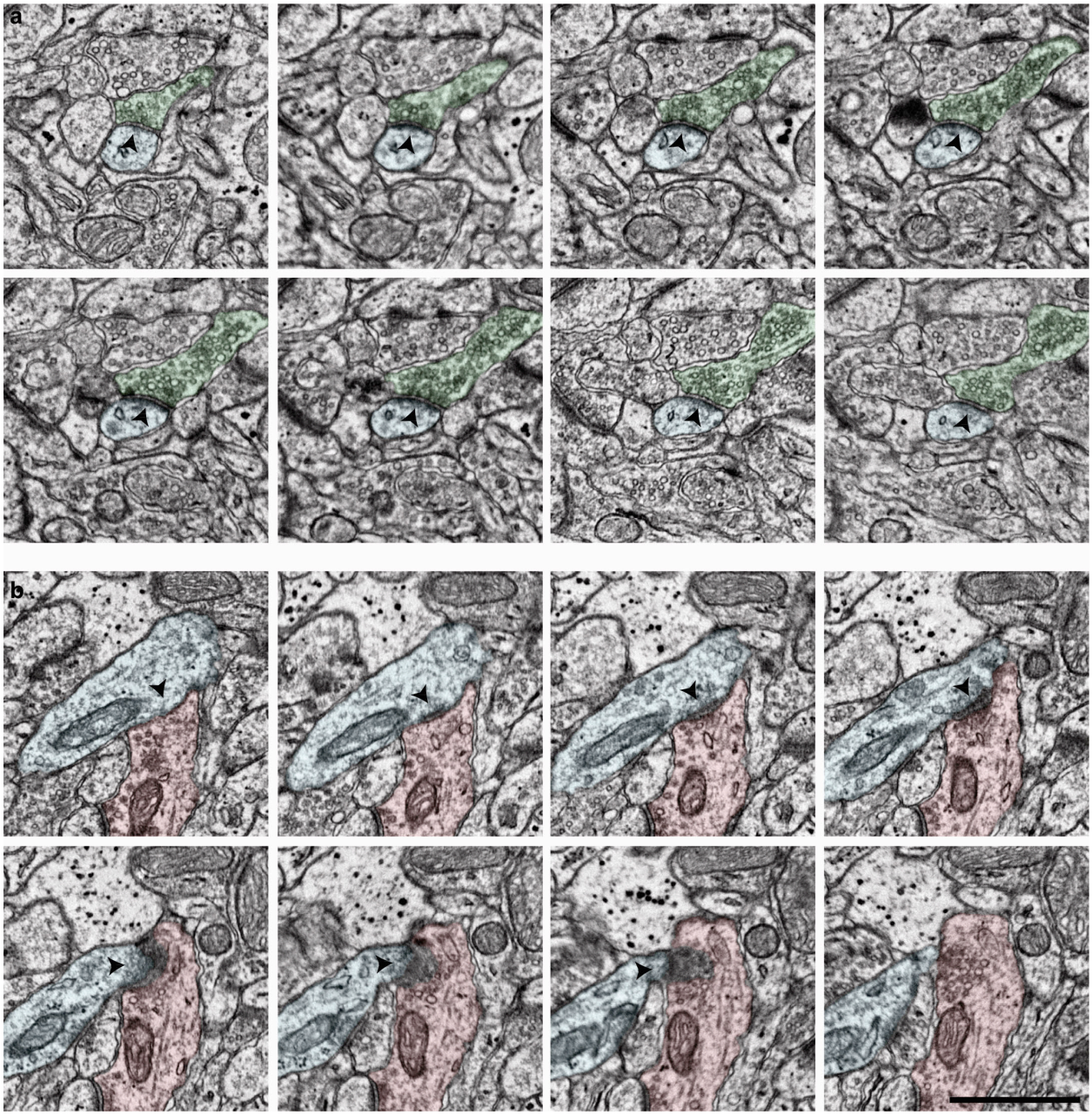


**Supplementary Figure 5. EM of synapses onto a convergence target.** Electron micrographs from 8 serial sections showing the synapse from **(a)** cell 4 (green) and **(b)** cell 10 (red) onto the dendritic shaft of a convergence target (cyan; same target as in Figure 4). Arrowheads point to the asymmetric synapses participating in the convergence. Scale bar, 1 μm.

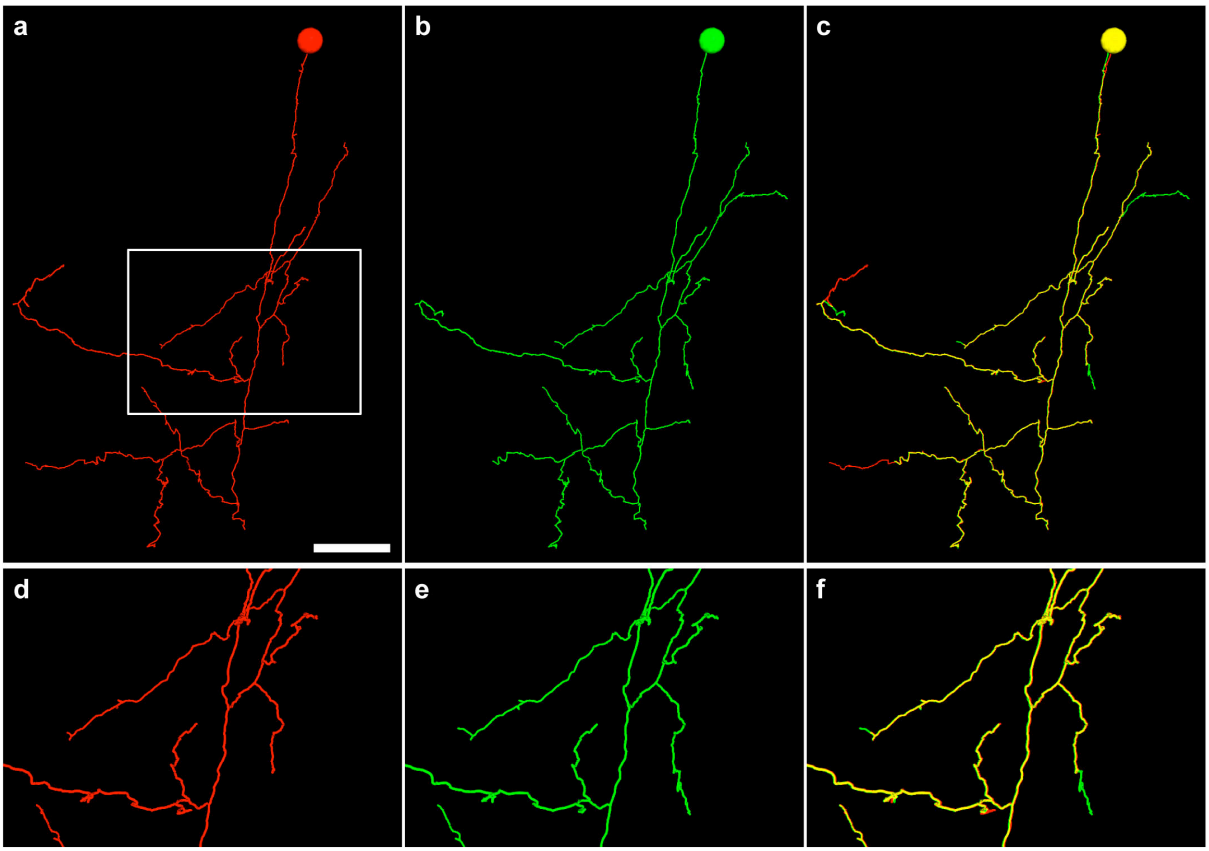


**Supplementary Figure 6. Independent verification of tracing.** The same axon was independently reconstructed by two individuals. **a,** 3-D rendered view of the reconstruction of the whole axon by the first individual. **b,** The reconstruction by the second individual. **c,** Overlay of the two reconstructions. Note that the core of the axon reconstruction is the same between tracings. **d-f,** Zoom in of the regions outlined in *a-c*, respectively. Scale bar, 10 μm in *a-c* and 30 μm in *d-f*.

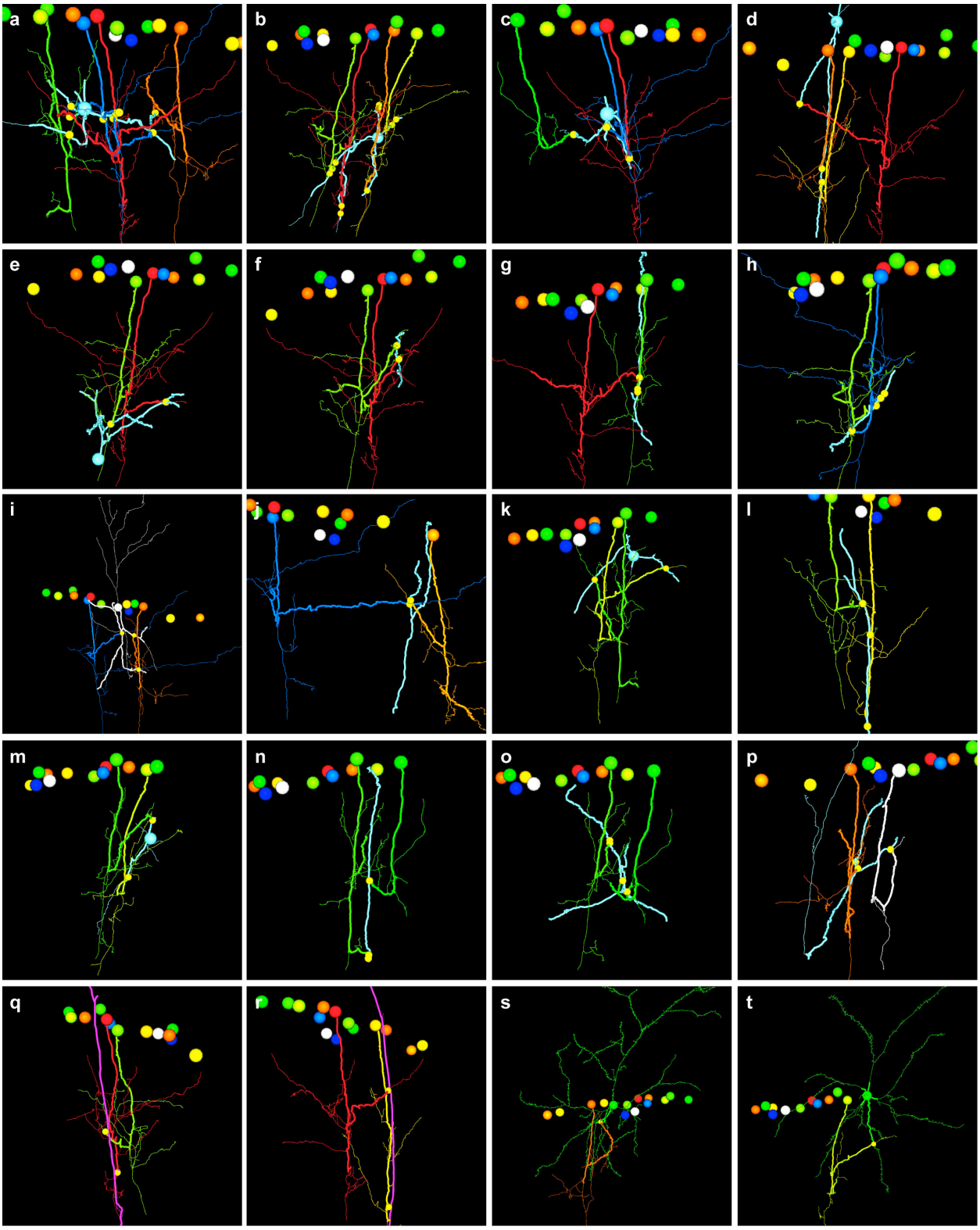


**Supplementary Figure 7. Connections between and convergences of functionally characterized cells.** Three-dimensional renderings of postsynaptic convergence

targets with participating presynaptic axons. Eleven postsynaptic inhibitory targets received 2 convergent inputs; 2 received 3 inputs, and 2 received 4 inputs. Additionally, 2 excitatory targets received convergent input, 2 characterized excitatory cells were interconnected, and one inhibitory target received convergent input from characterized excitatory and inhibitory neurons. **(a-o)** Examples of excitatory convergences onto inhibitory postsynaptic targets (cyan). **(p)** Example of excitatory and inhibitory convergence onto an inhibitory target. **(q-r)** Examples of excitatory convergences with excitatory targets (magenta). **(s-t)** Examples of interconnections between functionally characterized cells. Large balls represent cell bodies in the functionally imaged plane. Wire-frame models of the axons of presynaptic neurons participating in the convergences are shown descending from their cell bodies and making synapses (small yellow balls) onto their target as in Fig. 4a. Cell bodies and axons in the functionally imaged plane are coloured by orientation preference as in Fig. 1b. Outside the functionally imaged plane, inhibitory targets are cyan, and excitatory targets are magenta. Axons and dendrites were independently verified by a second individual blind to the original segmentation (thick tracing). Views are from different positions to improve visualization of convergence anatomy. The cell body spheres in the functionally imaged plane were standardized to 9.8 μm in diameter.

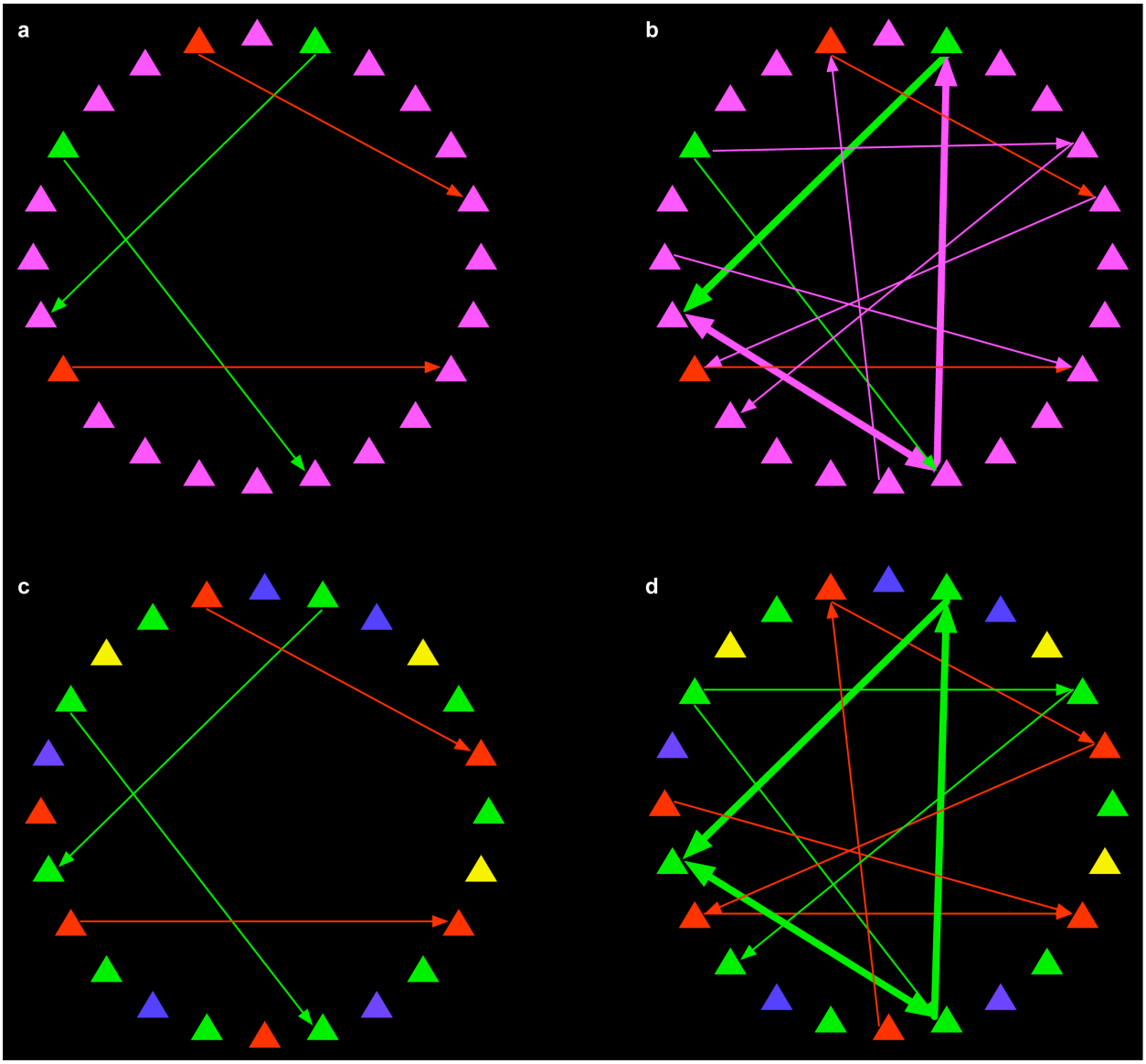


**Supplementary Figure 8. Schematic of connectivity patterns emerging with increasing numbers of physiologically characterized and segmented cells. a,** Sparse physiology and reconstruction. **b,** With denser reconstruction a network motif emerges (triangle of thick arrows). **c,** With more physiologically characterized cells the functional specificity of the connectivity in *a* is revealed. **d,** Denser reconstruction plus more physiologically characterized cells. The functional specificity of the motif in *b* is revealed. Cell colour in this figure corresponds to variation of an arbitrary functional property.